Evaluation of J-integral 2D

This is the derivation of the J-Integral for the 2D case. In our case the crack front is not curved; however, the indenter and free surface result in variation in the stress field along the crack which makes the problem 3D. That being said, every specimen designed to get a stress intensity factor also has 3D effects and it is unclear if the 3D effects are substantial at the point of maximum dissipation, i.e. directly under the indenter tip. Regardless, it is worth understanding the 2D formulism before discussing the details of evaluating the 3D integral as the 3D integral is just a scheme to approximate the pointwise (2D) energy release rate. In the context of quasi-static analysis, the J-integral is defined in two dimensions as

$$J = \lim_{\Gamma \to 0} \int_{\Gamma} \mathbf{H} \cdot \mathbf{n} \cdot \mathbf{q} d\Gamma \tag{1.1}$$

where Γ is a contour beginning on the bottom crack surface and ending on the top surface. The limit as $\Gamma \to 0$ indicates that Γ shrinks onto the crack tip and tractions on the crack are ignored, $\mathbf{q}$ is a unit vector in the direction of crack extension and $\mathbf{n}$ is the outward normal to Γ. $\mathbf{H}$, which is the Eshelby's energy-momentum tensor is given for small strains by

$$\mathbf{H} = W\mathbf{I} - \boldsymbol{\sigma} \cdot \frac{\partial \mathbf{u}}{\partial \mathbf{x}}. \tag{1.2}$$

For a linear elastic material, W is just the elastic strain energy density and no integral is needed in its evaluation; furthermore, there is no dependence on $\mathbf{x}$ i.e. we don't have a graded material. Proper evaluation of (1.2) requires that W is calculated using linear strains. To write (1.2) in terms of finite strains, the right hand term would be written in terms of the engineering Piola-Kirchoff stress and the deformation gradient. We can recast (1.1) in terms of the problem shown in Figure 1 and the integral becomes

$$J = -\oint_{C_1 + C_+ + \Gamma + C_-} \mathbf{H} \cdot \mathbf{m} \cdot \bar{\mathbf{q}} dC - \oint_{C_+ + C_-} \mathbf{t} \cdot \frac{\partial \mathbf{u}}{\partial \mathbf{x}} \cdot \bar{\mathbf{q}} dC \tag{1.3}$$

where $\mathbf{t}$ is the traction on the crack faces and $\bar{\mathbf{q}}$, which is an arbitrary smooth weighting function with the region enclosed $C_1 + C_+ - \Gamma + C_-$, is equal 1 on Γ and equal 0 on C_1. The equivalency of (1.1) and (1.3) can be understood in that $\bar{\mathbf{q}}$ is chosen such that if the contours were evaluated C_1 would disappear and as Γ is shrunk onto the crack tip the, contribution to the contour integral $C_+ + C_-$ when there is a traction on the surface of the crack vanishes.

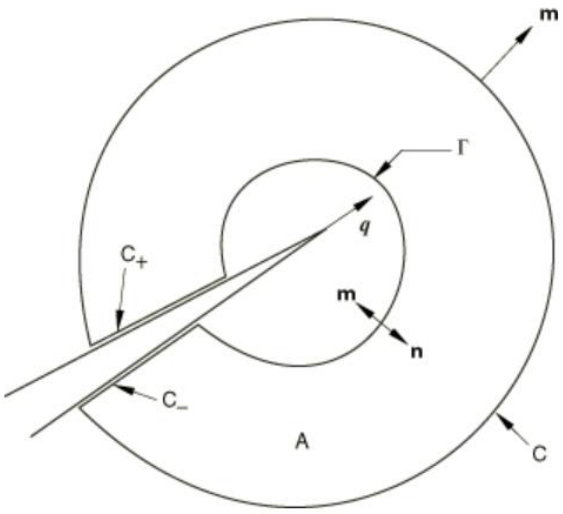

Figure 1. Closed contour $C + C_+ + \Gamma + C\_$ enclosed a domain A that includes the crack-tip region as $\Gamma \to 0$.

Applying the divergence theorem and assuming the crack surface is traction free we get the classical result for 2D

$$J = -\int_A \nabla \cdot \mathbf{H} \cdot \bar{\mathbf{q}} dA =$$

$$J = -\int_A \left[\nabla \cdot \left(W\mathbf{I} - \boldsymbol{\sigma} \cdot \frac{\partial \mathbf{u}}{\partial \mathbf{x}} \right) \cdot \bar{\mathbf{q}} + \mathbf{H} : (\nabla \cdot \bar{\mathbf{q}}) \right] dA$$

$$J = -\int_A \left[\left(\cancel{\nabla \cdot W\mathbf{I}} - \nabla \cdot \boldsymbol{\sigma} \cdot \frac{\partial \mathbf{u}}{\partial \mathbf{x}} - \cancel{\boldsymbol{\sigma} \cdot \nabla \cdot \frac{\partial \mathbf{u}}{\partial \mathbf{x}}} \right) \cdot \bar{\mathbf{q}} + \mathbf{H} : (\nabla \cdot \bar{\mathbf{q}}) \right] dA$$

$$J = \int_A \left(\boldsymbol{\sigma} \cdot \frac{\partial \mathbf{u}}{\partial \mathbf{x}} - W\mathbf{I} \right) : (\nabla \cdot \bar{\mathbf{q}}) dA \tag{1.4}$$

$$J = \int_A \left(\sigma_{ij} u_{j,k} - W \delta_{ki} \right) \bar{q}_{k,i} dA$$

Assuming equilibrium and no body forces:

$$\nabla \cdot \boldsymbol{\sigma} = 0$$

We are only interested in the crack along its propagation direction and (1.4) is simplified for our geometry to

$$J = \int_A \left(\sigma_{ij} \cdot u_{j,2} - W \delta_{2i} \right) q_{2,i} dA \tag{1.5}$$

which is the result of (Shih et al., 1986) in the absence of thermal strain, body force and crack face traction.

Evaluation of J-integral 3D

In 3D we are concerned with the pointwise energy release along a crack front which for just the second component of J has the form

$$J(s)=\lim_{\Gamma\to 0}\int_{\Gamma}\left(\sigma_{ij}u_{j,2}-W\delta_{2i}\right)n_i dC \tag{1.6}$$

and is schematically shown in figure 2.

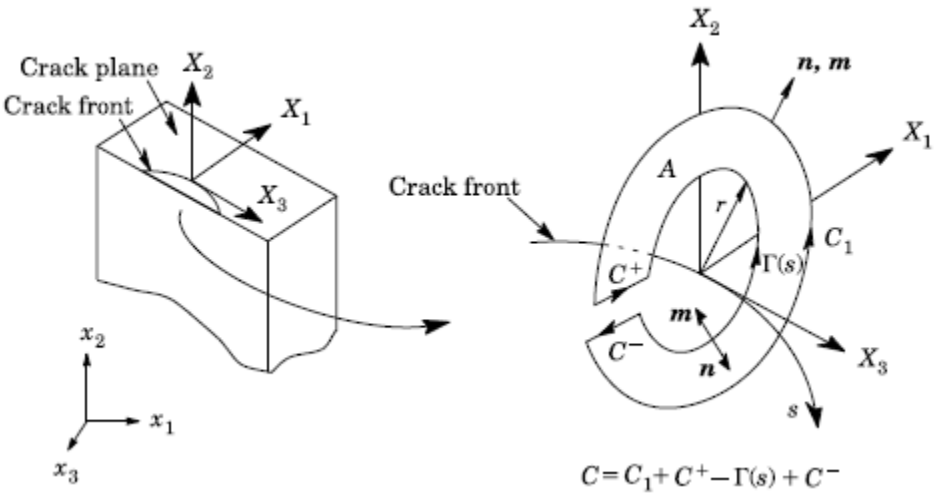

Figure 2. Schematic of $\Gamma(s)$ *in* (1.6). Schematic showing the relation of the problem to (1.4).

Note that the gradient terms in (1.6) are with respect to the local frame pictured in Figure 2; however, we consider a straight crack front in our analysis and global frame coincides with the local frame.

In general, the vector integral is

$$J(s)=J_k(s)v_k(s)=\lim_{\Gamma\to 0}\int_{\Gamma}\left(\sigma_{ij}u_{j,k}-W\delta_{ki}\right)m_i v_k dC \tag{1.7}$$

where $m_i=-n_i$ on $\Gamma(s)$ and v_k is the unit normal to the crack-front at position s.

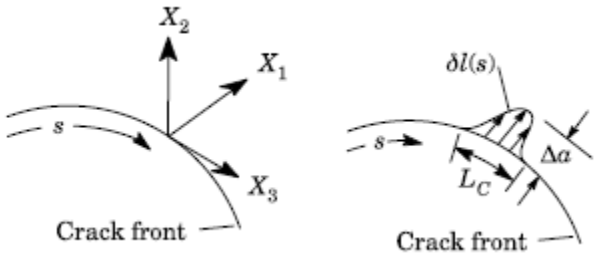

Figure 3. Virtual crack advance in the local X1-X3 plane at crack-front location s. Crack advance occurs in the X1-direction though in our case X2 is the direction of crack extension which is defined as in (1.8).

Consider a virtual displacement applied along the crack segment as pictured in Figure 3.

$$\delta l(s)=\Delta a l_k(s)v_k(s) \tag{1.8}$$

Here Δa is the amplitude of an arbitrary displacement $l_k(s)$ in the $v_k(s)$ direction. To first order, the energy release due to crack advance given in (1.8) is

$$-\delta\pi = \bar{J}\Delta a = \int_{L_c} J(s)\delta l(s)\,ds = \Delta a \int_{L_c} J(s) l_k(s) v_k(s)\,ds. \tag{1.9}$$

where $\bar{J}$ is the energy released when crack segment L_C advances by $\delta l(s)$. Substituting in (1.7) we get

$$\bar{J}\Delta a = \Delta a \int_{L_c} l_k(s) v_k(s) \left[\lim_{\Gamma\to 0} \int_{\Gamma} \left(\sigma_{ij} u_{j,k} - W\delta_{ki} \right) m_i v_k\, dC \right] ds. \tag{1.10}$$

Combining the integrals is akin to extruding the contour into a surface, S_t, which is a cylinder surrounding the crack front

$$\bar{J}\Delta a = \Delta a \lim_{\Gamma\to 0} \int_{S_t} \left(\sigma_{ij} u_{j,k} - W\delta_{ki} \right) l_k m_i\, dS \tag{1.11}$$

wherein we note for completeness that v_k is removed because the dot product of a unit vector with itself is unity. Following the 2D formulism, we create an enclosed volume , V , as pictured in Figure 4 and introduce a smooth vector field q which is l_k at S_t and 0 on S_1, S_2, S_3 and rewrite (1.11) assuming no surface tractions as

$$\bar{J} = \int_{S} \left(\sigma_{ij} u_{j,k} - W\delta_{ki} \right) q_k m_i\, dS. \tag{1.12}$$

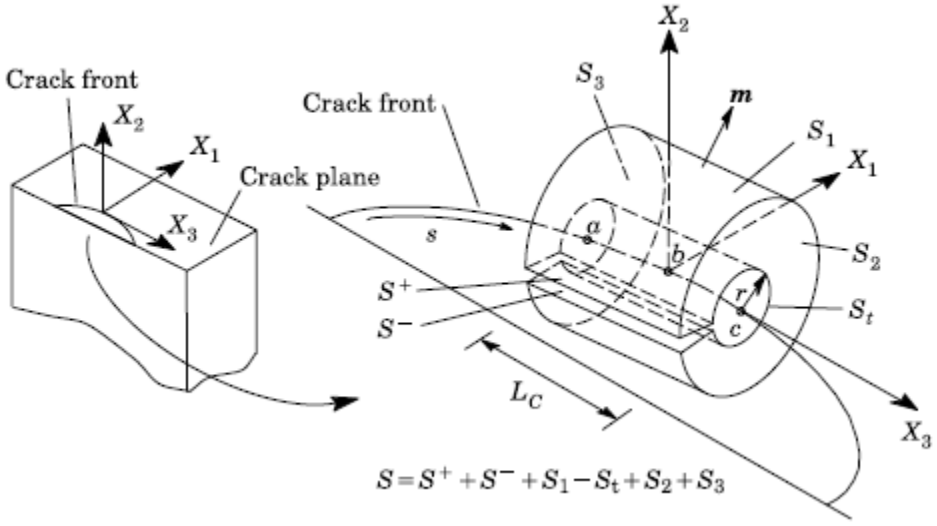

Figure 4

Applying the divergence theorem and assuming the divergence of the momentum tensor is 0, we obtain

$$\bar{J} = \int_V \left(\sigma_{ij} u_{j,k} - W \delta_{ik} \right) q_{k,i} dV. \tag{1.13}$$

Finally, we would like to relate $\bar{J}$ to $J(s)$ by assuming $J(s)$ does not vary significantly over the interval L_C. Rearranging (1.9) we get

$$J(s) = \frac{\bar{J}}{\int_{L_c} l_k(s) v_k(s) ds}. \tag{1.14}$$

Evaluation of J-integral with phase boundaries in 3D

Consider the contours in figure 5 at a position (s) along a crack front. The phase boundary contribution to the J integral in the absence of traction at the crack, body forces, and thermal strain is

$$J = \int_\Gamma \left(\sigma_{ij} u_{j,k} - W \delta_{ki} \right) n_i v_k dC - \int_{\Gamma_{pb}} \left(\sigma_{ij} u_{j,k} - W \delta_{ki} \right) z_i v_k dC. \tag{1.15}$$

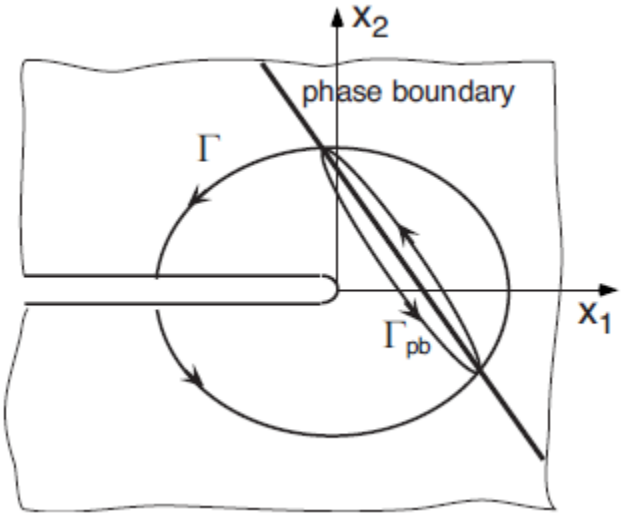

Figure 5. Contours for J-integral evaluation at a crack tip located near a phase boundary.

Reapplying the divergence theorem to (1.12) and keeping the divergence of the momentum tensor results in

$$\bar{J}_{tip} = \int_V \left(\sigma_{ij} u_{j,k} - W \delta_{ik} \right) q_{k,i} dV + \int_{V_{pb}} \left(\sigma_{ij} u_{j,k} - W \delta_{ik} \right)_{,i} q_k dV = \bar{J} + \bar{J}_{pb}. \tag{1.16}$$

where the second term is non-zero and contains the inhomogeneity, but also some of the contributions around the inhomogeneity. If the material gradients are smooth, then the second term must be evaluated as a volume integral in the 3D domain approach, in the case of a sharp, discontinuous interface, but otherwise homogenous medium, $\bar{J}_{pb} \to \bar{J}_{\text{int}}$ and needs to be treated as a surface integral

on the interface if the effects of the interface are to be isolated. Applying the divergence theorem in the opposite direction gives

$$\bar{J}_{\text{int}} = \int_{V_{pb}} \left(\sigma_{ij} u_{j,k} - W\delta_{ik}\right)_{,i} q_k dV = \int_{\Sigma} \left(\sigma_{ij} u_{j,k} - W\delta_{ik}\right) l_k z_k dS \tag{1.17}$$

Note that z_k is the unit surface normal which is taken to be positive in the crack propagation direction, and we drop part of the functional dependence on q_k. Mainly, the line contour to area integral equivalency used to reformulate (1.11) into (1.12) is not applicable and we leave the weighted evaluation along the crack front such that (1.14), (1.16), and (1.17) can be written as

$$J(s) = \frac{\bar{J}_{tip}}{\int_{L_c} l_k(s) v_k(s) ds}. \tag{1.18}$$

Numerical integration of the J integral

The numerical integration of (1.18) is performed using shape functions of the C3D20 elements. Consistent with the isoparametric formulation, we take q_2 within an element as

$$q_2 = \sum_{i=1}^{20} h^i q_2^i. \tag{1.19}$$

On S_t $q_2^i = l_2$ and on S_1, S_2, S_3 $q_2^i = 0$, but in-between the boundaries q_2^i is between 0 and 1. A number of options for the shape of the virtual crack growth can be chosen. We choosing to evaluate $J(s)$ at node M using a piecewise linear function as shown in Figure 6. The choice considers contributions to the release rate at the node from its surrounding elements. We do not evaluate $J(s)$ at the mid side nodes like Abaqus does. For quadratic elements and setting a mid-node to be zero, q must become negative between M-1 and M+1 and the mid nodes. Thus, the value of $J(s)$ will be slightly higher than it should be, but the spatial averaging along the crack front will be minimized. The spatial averaging under the indenter is a secondary effect there is no need for a more complicated script that evaluates computes $J(s)$ at the mid-nodes.

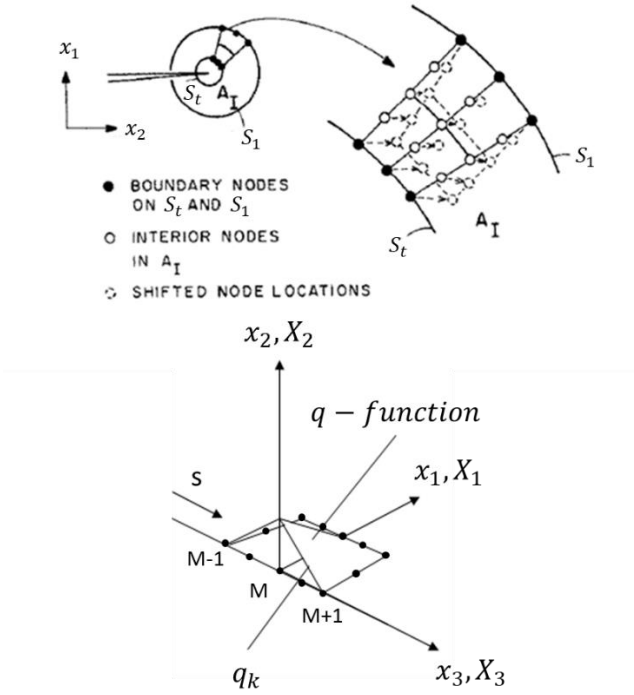

Figure 6. (top) is a schematic showing a linearly decreasing virtual shift of nodes in the 2 direction between S1 and St for the node set corresponding to M. (bottom) is a schematic showing how q varies along the crack.

Some care needs to be given to the choice of q_2 between the contour regions, especially when the mesh is poor in some areas. The most accurate results will be from regions where the mesh quality is high, structured, and away from the crack tip. Here we choose q to be a linear function between the inner contour and outer contour surfaces e.g. see Figure 6 example for how q would be defined for the first ring of elements.

The gradient of q is computed at the gauss integration points using shape functions.

$$\frac{\partial q_2}{\partial x_j} = \sum_{i=1}^{20} \frac{\partial h_i}{\partial x_j} q_{2i} = \sum_{i=1}^{20} \sum_{k=1}^{3} \frac{\partial h_i}{\partial r_k} \frac{\partial r_k}{\partial x_j} q_{2i} = \sum_{i=1}^{20} \sum_{k=1}^{3} \frac{\partial h_i}{\partial r_k} J_{kj}^{-1} q_{2i}. \tag{1.20}$$

Similarly, the gradient of displacement is given by

$$\frac{\partial u_i}{\partial x_2} = \sum_{k=1}^{20} \sum_{m=1}^{3} \frac{\partial h_k}{\partial r_m} J_{mj}^{-1} u_{ik}. \tag{1.21}$$

For the surface and line integral, q is interpolated to gauss integrations points in the interface plane or crack front. In the next section, details of the integration procedure are given in terms of a transformation of the 3D shape functions. Mainly, we use for the line integral 2 Gaussian integration points, for surface integrals 3x3 Gaussian integration scheme, and for the volume integrals we use a 3x3x3 Gaussian integration. The discretized form of the domain expression for the energy release rate (1.5) is

$$\bar{J} = \sum_{\substack{\text{all}\\ \text{elements}\\ \text{in V}}} \sum_{p=1}^{27} \left\{ \left(\sigma_{ij} \frac{\partial u_j}{\partial x_2} - W\delta_{2i} \right) \frac{\partial q_2}{\partial x_i} \det(\mathbf{J}) \right\}_p w_p + \sum_{\substack{\text{all}\\ \text{interfaces}\\ \text{in V}}} \sum_{p=1}^{9} \left\{ \left(\frac{\left(\sigma_{ij}^+ + \sigma_{ij}^-\right)}{2} \left(\frac{\partial u_j^+}{\partial x_2} - \frac{\partial u_j^-}{\partial x_2} \right) - \left(W^+ - W^-\right)\delta_{2i} \right) l_2 z_2 \det\left(\mathbf{J}_{\textit{surface element}}\right) \right\}_p w_p \tag{1.22}$$

The integral in the denominator of (1.18) is evaluated between M-1 and M and between M and M+1 as

$$\begin{aligned} \int_{M-1}^{M+1} l_k(s) v_k(s)\, ds &= \int_{-1}^{1} \frac{1+t}{2} \det(J_{line})\, dt + \int_{-1}^{1} \frac{1-t}{2} \det(J_{line})\, dt \\ &= \sum_{p=1}^{2} \left\{ \frac{1+t}{2} \det(J_{line}) \right\}_p w_p + \sum_{p=1}^{2} \left\{ \frac{1-t}{2} \det(J_{line}) \right\}_p w_p . \end{aligned} \tag{1.23}$$

In the case M is evaluated at a surface, the integral (1.23) becomes

$$\int_{M-1}^{M} l_k(s) v_k(s)\, ds = \int_{-1}^{1} \frac{1+t}{2} \det(J_{line})\, dt = \sum_{p=1}^{2} \left\{ \frac{1+t}{2} \det(J_{line}) \right\}_p w_p . \tag{1.24}$$

The simple functional form of $l_k(s)$, the straight crack front, and small strains lend itself to a simple trapezoidal numerical integration in cartesian reference coordinates.

Isoparametric formulization for C3D20 element

General concepts

The basic idea of isoparametric finite element formulation is to achieve the relationship between element displacements at any point and the element nodal point displaces directly through the interpolation (shape) functions. For a general three-dimensional element, the coordinate interpolations are

$$\begin{aligned} x(\mathbf{r}) &= \sum_{i=1}^{q} h_i(\mathbf{r})\, x_i \\ y(\mathbf{r}) &= \sum_{i=1}^{q} h_i(\mathbf{r})\, y_i \\ z(\mathbf{r}) &= \sum_{i=1}^{q} h_i(\mathbf{r})\, z_i \end{aligned} \tag{1.25}$$

where $\mathbf{x} = \{x, y, z\}$ are the global coordinate components at any point of the element with local (natural) coordinates $\mathbf{r} = \{r, s, t\}$, and $x_i, y_i, z_i, i = 1, \ldots, q$, are the coordinates of the q element nodes in global coordinates. The interpolation functions h_i are defined in the element natural coordinates r, s, and t respectively. The natural coordinates vary from $+1$ to -1, thus the location of element nodes

in the natural and global coordinate systems are available and natural coordinates are in the appropriate interval for gaussian quadrature. The fundamental property of the interpolation function is that h_i is unity at node i and zero at all other nodes.

Similar to coordinates, the displacements are defined as

$$\begin{aligned} u(\mathbf{r}) &= \sum_1^q h_i(\mathbf{r}) u_i \\ v(\mathbf{r}) &= \sum_1^q h_i(\mathbf{r}) v_i \\ w(\mathbf{r}) &= \sum_1^q h_i(\mathbf{r}) w_i \end{aligned} \tag{1.26}$$

where $\mathbf{u} = \{u, v, w\}$ are the displacements at any point of the element in global coordinates, and $u_i, v_i, w_i, i = 1, \ldots, q$, are the displacements of the q element nodes in the global coordinate system. The transformation from local to global system for derivatives will be discussed later. The Abaqus node ordering and local frame is schematically presented in figure 7.

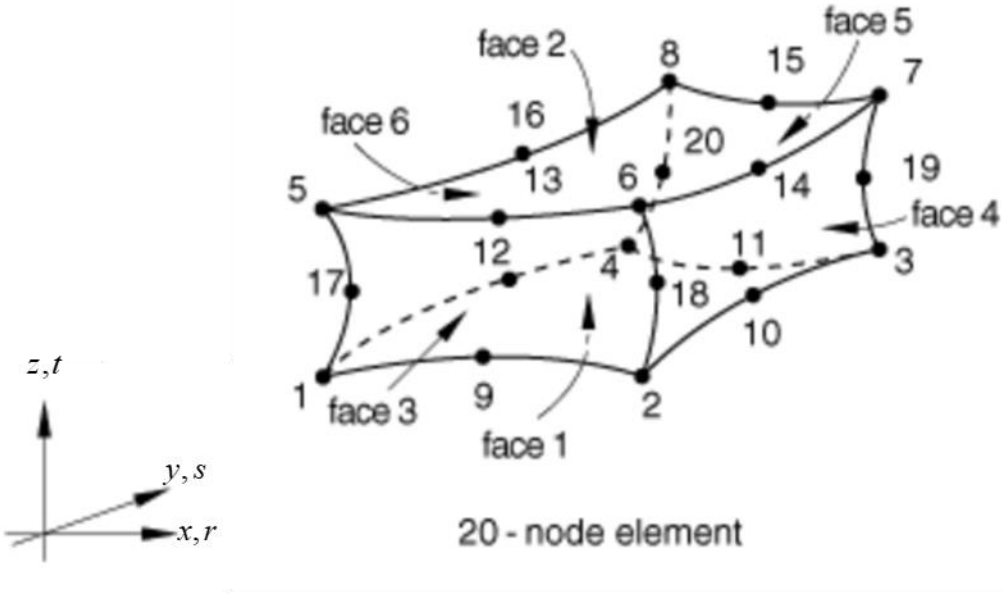

Figure 7. Node ordering, frame, and face labeling from abaqus manual .

Using the node ordering presented in Figure 7 the shape functions can be constructed by inspection:

$$\begin{aligned} h_1 &= g_1 - (g_9 + g_{12} + g_{17})/2 & h_6 &= g_6 - (g_{13} + g_{14} + g_{18})/2 \\ h_2 &= g_2 - (g_9 + g_{10} + g_{18})/2 & h_7 &= g_7 - (g_{14} + g_{15} + g_{19})/2 \\ h_3 &= g_3 - (g_{10} + g_{11} + g_{19})/2 & h_8 &= g_8 - (g_{15} + g_{16} + g_{20})/2 \\ h_4 &= g_4 - (g_{11} + g_{12} + g_{20})/2 & h_i &= g_i \text{ for } i = 9, \ldots, 20 \\ h_5 &= g_5 - (g_{13} + g_{16} + g_{17})/2 \end{aligned} \tag{1.27}$$

where

$$
\begin{aligned}
&g_i = 0 \text{ if node is not present} \\
&g_i = G(r, r_i)G(s, s_i)G(t, t_i) \\
&G(\beta, \beta_i) = \frac{1}{2}(1 + \beta\beta_i), \text{ for } \beta_i = \pm 1 \\
&G(\beta, \beta_i) = \frac{1}{2}(1 - \beta^2), \text{ for } \beta_i = 0 \text{ (mid nodes)} \\
&\beta = r, s, t
\end{aligned}
\tag{1.28}
$$

The shape functions for the C3D20 using the node labeling convention in figure 7 are explicitly written as

$$
\begin{aligned}
h_i &= \frac{1}{8}\left(1 + \beta_i^r r\right)\left(1 + \beta_i^s s\right)\left(1 + \beta_i^t t\right)\left(\beta_i^r r + \beta_i^s s + \beta_i^t t - 2\right), \text{ corners } i = 1, \ldots, 8 \\
h_i &= \frac{1}{4}\left(1 - r^2\right)\left(1 + \beta_i^s s\right)\left(1 + \beta_i^t t\right), \; i = 9, 11, 13, 15 \\
h_i &= \frac{1}{4}\left(1 - s^2\right)\left(1 + \beta_i^r r\right)\left(1 + \beta_i^t t\right), \; i = 10, 12, 14, 16 \\
h_i &= \frac{1}{4}\left(1 - t^2\right)\left(1 + \beta_i^r r\right)\left(1 + \beta_i^s s\right), \; i = 17, 18, 19, 20.
\end{aligned}
\tag{1.29}
$$

The derivatives of these shape functions $\partial h_i / \partial \mathbf{r}$ are derived with respect to r as

$$
\begin{aligned}
\frac{\partial h_i}{\partial r} &= \frac{1}{8}\beta_i^r \left(1 + \beta_i^s s\right)\left(1 + \beta_i^t t\right)\left(2\beta_i^r r + \beta_i^s s + \beta_i^t t - 1\right) \text{ , corners } i = 1, \ldots, 8 \\
\frac{\partial h_i}{\partial r} &= -\frac{1}{2} r \left(1 + \beta_i^s s\right)\left(1 + \beta_i^t t\right), \; i = 9, 11, 13, 15 \\
\frac{\partial h_i}{\partial r} &= \frac{1}{4}\beta_i^r \left(1 - s^2\right)\left(1 + \beta_i^t t\right), \; i = 10, 12, 14, 16 \\
\frac{\partial h_i}{\partial r} &= \frac{1}{4}\beta_i^r \left(1 - t^2\right)\left(1 + \beta_i^s s\right), \; i = 17, 18, 19, 20.
\end{aligned}
\tag{1.30}
$$

with respect to s as

$$
\begin{aligned}
\frac{\partial h_i}{\partial s} &= \frac{1}{8}\beta_i^s \left(1 + \beta_i^r r\right)\left(1 + \beta_i^t t\right)\left(\beta_i^r r + 2\beta_i^s s + \beta_i^t t - 1\right), \text{ corners } i = 1, \ldots, 8 \\
\frac{\partial h_i}{\partial s} &= \frac{1}{4}\beta_i^s \left(1 - r^2\right)\left(1 + \beta_i^t t\right), \; i = 9, 11, 13, 15 \\
\frac{\partial h_i}{\partial s} &= -\frac{1}{2} s \left(1 + \beta_i^r r\right)\left(1 + \beta_i^t t\right), \; i = 10, 12, 14, 16 \\
\frac{\partial h_i}{\partial s} &= \frac{1}{4}\beta_i^s \left(1 - t^2\right)\left(1 + \beta_i^r r\right), \; i = 17, 18, 19, 20.
\end{aligned}
\tag{1.31}
$$

and with respect to t as

$$
\begin{aligned}
\frac{\partial h_i}{\partial t} &= \frac{1}{8}\beta_i^t\left(1+\beta_i^r r\right)\left(1+\beta_i^s s\right)\left(\beta_i^r r+\beta_i^s s+2\beta_i^t t-1\right), \text{ corners } i=1,\ldots,8\\
\frac{\partial h_i}{\partial t} &= \frac{1}{4}\beta_i^t\left(1-r^2\right)\left(1+\beta_i^s s\right),\ i=9,11,13,15\\
\frac{\partial h_i}{\partial t} &= \frac{1}{4}\beta_i^t\left(1-s^2\right)\left(1+\beta_i^r r\right),\ i=10,12,14,16\\
\frac{\partial h_i}{\partial t} &= -\frac{1}{2}t\left(1+\beta_i^r r\right)\left(1+\beta_i^s s\right),\ i=17,18,19,20.
\end{aligned}
\tag{1.32}
$$

To map the derivatives in the local coordinates to global coordinates or transform integrals from the global coordinate system to the local coordinate system, we need to build the Jacobian of the transformation in (1.25) and (1.26) using (1.30), (1.31), and (1.32)

$$
\mathbf{J}=\frac{\partial x_i}{\partial r_j}=\begin{bmatrix}\partial x/\partial r & \partial y/\partial r & \partial z/\partial r\\ \partial x/\partial s & \partial y/\partial s & \partial z/\partial s\\ \partial x/\partial t & \partial y/\partial t & \partial z/\partial t\end{bmatrix}
\tag{1.33}
$$

where each derivative is defined as

$$
\begin{aligned}
\frac{\partial x}{\partial r}&=\sum\frac{\partial h_i}{\partial r}x_i,\ \frac{\partial y}{\partial r}=\sum\frac{\partial h_i}{\partial r}y_i,\ \frac{\partial z}{\partial r}=\sum\frac{\partial h_i}{\partial r}z_i\\
\frac{\partial x}{\partial s}&=\sum\frac{\partial h_i}{\partial s}x_i,\ \frac{\partial y}{\partial s}=\sum\frac{\partial h_i}{\partial s}y_i,\ \frac{\partial z}{\partial r}=\sum\frac{\partial h_i}{\partial s}z_i\\
\frac{\partial x}{\partial t}&=\sum\frac{\partial h_i}{\partial t}x_i,\ \frac{\partial y}{\partial t}=\sum\frac{\partial h_i}{\partial t}y_i,\ \frac{\partial z}{\partial t}=\sum\frac{\partial h_i}{\partial t}z_i.
\end{aligned}
\tag{1.34}
$$

The derivatives for displacement and other quantities described by the shape functions can be constructed in the same manner.

An n-point gaussian integration is utilized in finite elements because it can be used to calculate the exact result of a polynomial function polynomials of degree 2n-1 or less by a suitable choice points r_i, s_i, t_i and weights w_i. The integral when taken exactly is expressed in the local coordinates as

$$
\int_{-1}^{1}\int_{-1}^{1}\int_{-1}^{1} f(r,s,t)drdsdt \approx \sum_{i=1}^{n}\sum_{j=1}^{m}\sum_{k=1}^{l} w_i w_j w_k f(r_i,s_j,t_k)=\sum_{p=1}^{nml} w_p f(r_p,s_p,t_p)
\tag{1.35}
$$

and the transform of the integrals from global coordinate systems to local coordinate system is

$$
dV = dxdydz = \det(\mathbf{J})drdsdt
\tag{1.36}
$$

The C3D20 element uses 3x3x3 gaussian integration (3 gauss points along each dimension) and the volume integral is exact for the tri-quadratic shape functions. The ordering of the integration points is shown in figure 8.

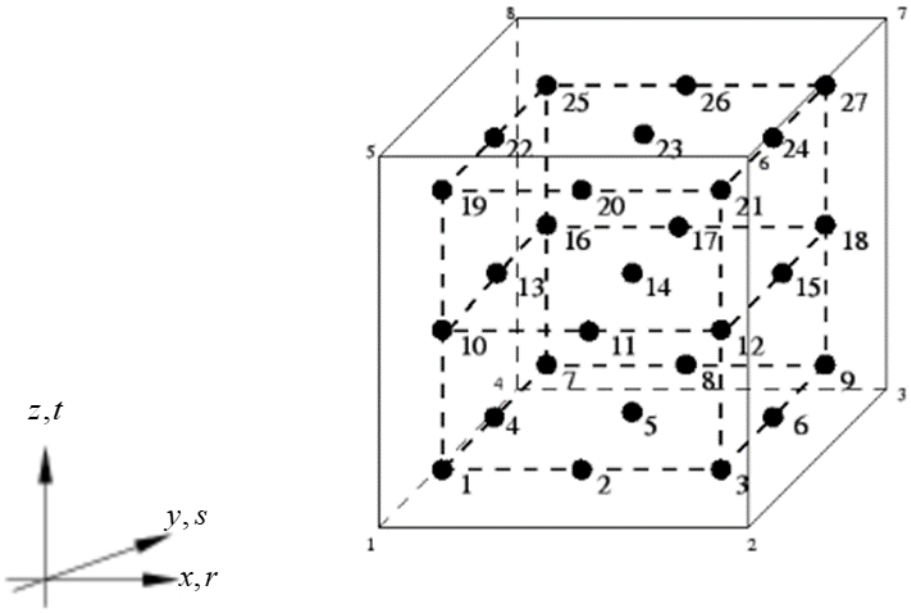

Figure 8. Integration point numbering for Abaqus C3D20 element taken from here.

The weights and locations of the gauss points for each dimension follow the 3-point Gauss rule and are summarized in Table 1 for the first three nodes and the derivation of the points can be found here. Matlab scripts for performing the Gauss integration can be found here starting page 12.

Table 1. Worked out example for 3D 3-point quadrature rule.

	Point 1	Point 2	Point 3
r w	$-\sqrt{3/5}$ $5/9$	0 $8/9$	$\sqrt{3/5}$ $5/9$
s w	$-\sqrt{3/5}$ $5/9$	$-\sqrt{3/5}$ $5/9$	$-\sqrt{3/5}$ $5/9$
t w	$-\sqrt{3/5}$ $5/9$	$-\sqrt{3/5}$ $5/9$	$-\sqrt{3/5}$ $5/9$

In the case that we wish to interpolate from Gauss points to nodes or to a surface we need to modify the basis of natural coordinates to the Gauss points. The problem is visualized in 2D in Figure 9. We observed based on Table 1 that when $\{\xi,\eta\}=\{1,1\}$, $\{r,s\}=\left\{\sqrt{\frac{3}{5}},\sqrt{\frac{3}{5}}\right\}$ and there a proportionality constant of $\sqrt{\frac{5}{3}}$. The variable β_i^s which denotes the location in natural coordinates of the value being extrapolated remains the same as before but the natural nodal coordinates which are usually less than

or equal to 1 become less than or equal to $\sqrt{\frac{5}{3}}$ (i.e. for node 3 in Figure 5, the nature coordinates are $\{\xi,\eta\}=\left\{\sqrt{\frac{5}{3}},\sqrt{\frac{5}{3}}\right\}$ and we replace $\{r,s,t\}$ in (1.29) with $\{\xi,\eta,\zeta\}$) .

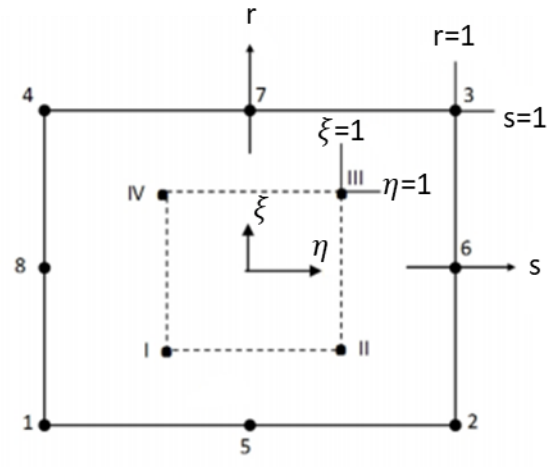

Figure 9. 2D schematic showing the two coordinate systems.

Unlike in the case of the 2x2x2 integration and the C3D8 element, 3x3x3 integration scheme means that the form of the shape functions in (1.29) is not valid for extrapolation from all of the integration points. We must create a mapping between the node convention and the integration point conventions in Figures 7 and 8 which is summarized in Table 2. Essentially, some integration points that would correspond to a face node or center node, are ignored.

Table 2. The mapping between element node ids (N) and corresponding integration point ids (GP) for extrapolation from integration point data.

N	1	2	3	4	5	6	7	8	9	10	11	12	13	14	15	16	17	18	19	20
GP	1	3	9	7	19	21	27	25	2	6	8	4	20	24	26	22	10	12	18	16

Transformation of 3D shape functions for boundary integrals

The strategy for accurate numerical integration on surfaces or edges is to extrapolate needed quantities to integration points on a surface or line that we want to perform integration on. Realizing that the order of the polynomial is simply taken as the product of variables, the degree of the polynomials in the shape function is 3 in the 2D case of bi-quadratic shape functions and the number of gauss point for exact integration is at least a 2x2 grid. In the case of a line integral 2 gauss points are needed because the order is 2. The integral transforms from 3D (1.35) to 2D area integrals and 1D line integrals are based on simple calculus and are presented as follows: for the 2D case assuming ds=0, the integral is given as

$$\int_S f\left(x,y,z\right)dS = \int_{-1}^{1}\int_{-1}^{1} f\left(x(r,s,t),y(r,s,t),z(r,s,t)\right)\left\|\begin{matrix}\frac{\partial x}{\partial r} & \frac{\partial x}{\partial t}\\ \frac{\partial y}{\partial r} & \frac{\partial y}{\partial t}\\ \frac{\partial z}{\partial r} & \frac{\partial z}{\partial t}\end{matrix}\right\| drdt \tag{1.37}$$

and for a line assuming dr=ds=0 as

$$\int_L f\left(x,y,z\right)dL = \int_{-1}^{1} f\left(x(r,s,t),y(r,s,t),z(r,s,t)\right)\left\|\begin{matrix}\frac{\partial x}{\partial t}\\ \frac{\partial y}{\partial t}\\ \frac{\partial z}{\partial t}\end{matrix}\right\| dt. \tag{1.38}$$

The quantities needed to compute these integrals are available from the general shape functions and their derivatives.

Example 1 – Through crack in infinite plate

Analytical solution

To verify the 3D J-integral procedure in the absence of interfaces, a simpler, well know problem of an through thickness crack in an infinite plate under uniaxial stress is utilized.

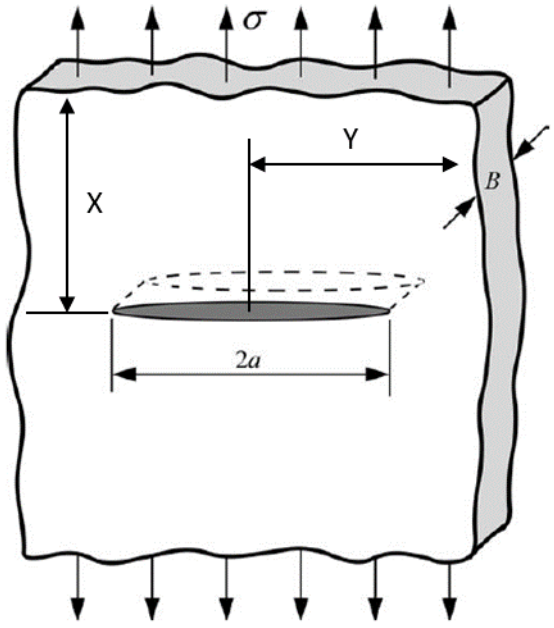

Figure 10. A schematic showing problem to be modeled.

The analytical solution for the problem for K_I stress intensity factor is simply

$$K_I = \sigma\sqrt{\pi a}\ . \tag{1.39}$$

Model definition

Table 1. Model parameters.

a	X	Y	B	σ	E (GPa)	ν
0.5	6	4	4	10000	200	0.32

Model parameters are summarized in Table 1. Symmetry is utilized to create a 1/8th model and C3D20 elements are utilized at and around the crack with nodes collapsed to create a singularity. The mesh was designed so that around the crack there are 10 rings of elements (See Figure below).

Results

For the applied stress there is no difference between finite and small strain formulation results for K_I. Similarly, there is no difference if full or half precision (default) is used to store stress and displacement in the output database. Perhaps precision matters when computing interface quantities; this will be explored in the next section. Increasing the applied stress only scales the computed quantities as expected.

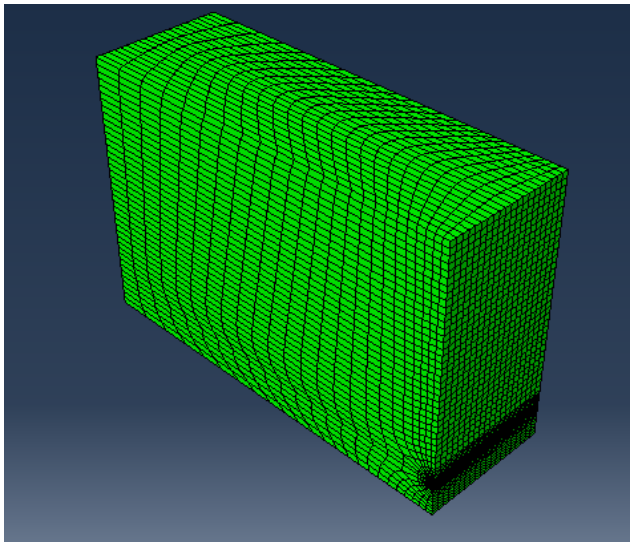

Figure 11. Model design.

Table 1. Summary of calculated K_I and J for through crack in infinite plate. The analytical solution $K_{I,Analytical}$ for the geometry and loading is 12533.

Contours	0	2	4	12	% Error from $K_{I,Analytical}$ (contour 4)
$K_{I,Abaqus}$	12428	12677	12677	12677	1.15%
K_I	12438	12689	12689	12688	1.24%

J_{Abaqus}	6.932E-4	7.212E-4	7.213E-4	7.213E-4	-
J	6.943E-4	7.227E-4	7.227E-4	7.225E-4	-

The results are summarized in Table 1. The analytical solution for K_I is 12533 and the percent error for our implementation is 1.24% and the percent difference in K_I computed by Abaqus and our code is just 0.094%. The error from the analytical solution went from 3.4% to 1.24% when X was changed from 3 to 6 and the difference may go down by increasing the model size. The agreement between Abaqus and our calculation is excellent. The small difference can be attributed to choosing a more convenient interval when computing (1.14).

Example 2 – Crack in front of Interface in a Compact tension specimen

Model design

A crack in-front of a sharp interface for a 2D plane strain compact tension (CT) specimen is explored in (Simha et al., 2005) and follows the recommended relative dimensions of ASTM E647. The model is picture below in Figure 12.

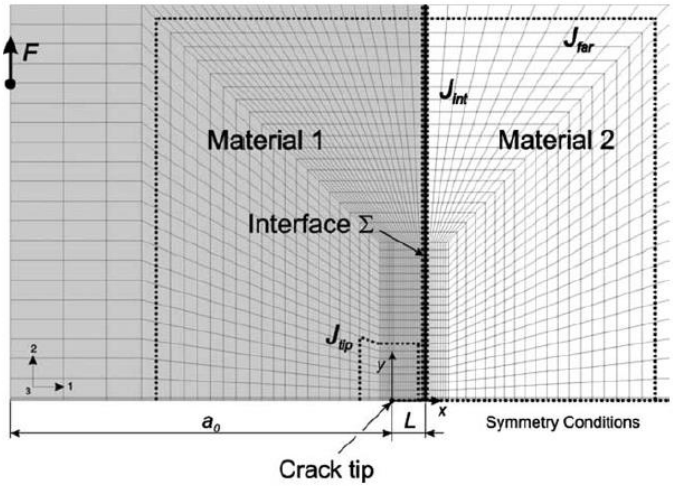

Figure 12. Picture of crack in front of sharp interface (Simha et al., 2005).

The critical geometry and material properties reported in (Simha et al., 2005) are summarized in Table 1.

Table 1. Model parameters for the 2D model.

a_o	L	E1 (GPa)	$\nu 1$	E2 (GPa)	$\nu 2$
29	0.6	70	0.3	210	0.3

A 3D model with the same critical geometry was create after ASTM E647 recommend geometry and is pictured in Figure 13. Symmetry is applied out-of-plane and in-front of the crack front, and a traction is applied to the ring to load the specimen in a realistic manner.

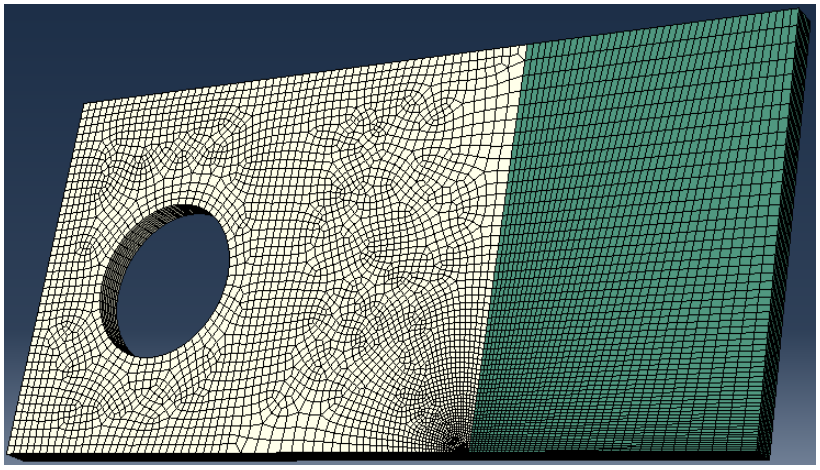

Figure 13. 3D model geometry for a CT specimen. The green mesh is material 2.

Results

The inhomogeneity contribution to the J integral from the sharp interface can be evaluated as

$$J_{tip} = J_{far} + J_{Int}. \tag{1.40}$$

For the geometry and material properties (Simha et al., 2005) report $J_{tip} = 0.44 J_{far}$ and for our 3D model we similarly get $J_{tip} = 0.438 J_{far}$ after an arbitrary 45 contour levels. Given the unstructured mesh, the 3D effects, and lack of saturation in J_{far} this is an excellent result.

To demonstrate the interface contribution to J integral is appropriately calculated we plot in Figure 14 J_{tip} calculated using (1.40) and J_{far} vs the contours where each contour adds a layer of elements, thereby interacting with more of the interface. The maximum error which occurs where the gradient of the inhomogeneity is the largest and the mesh is not highly structured results in a percent error in K_I of 0.44%. At larger number of contours the error is on the order of 0.02% from the J_{tip} solution close to the crack tip. It looks like the ratio of J_{tip} to J_{far} may rise with more contours since J_{far} doesn't appear to have completely saturated.

As long as interface sets are appropriately handled, the methodology can be extended to the many interface cases and the results will be representative of the physical phenomena at play.

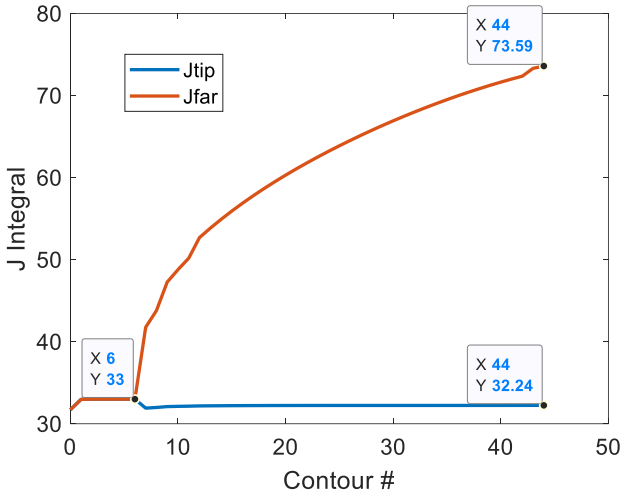

Figure 14. Path independence by considering the inhomogeneity of the interface.

Example 3 – Spherical Indentation of three-point bend specimen

The third and final example is of the spherical indentation of a three-point bend specimen pictured in Figure 15.

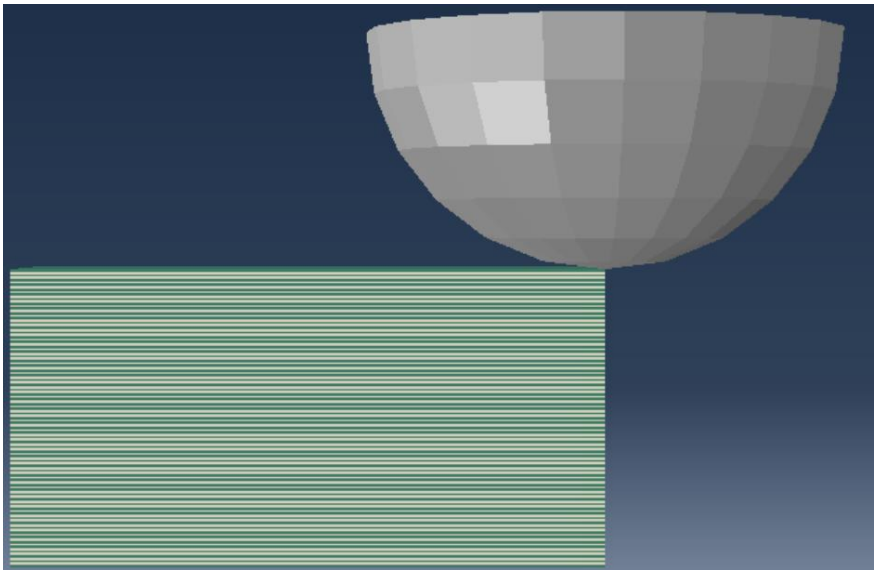

Figure 15. Spherical indentation of quarter model with crack.

In Figure 16, the solutions at the tip and far away from the tip are compared. Noticeably, path independence is achieved up to 21 contours; after which the integral far from the tip begins to diverge from the near tip solution. We can apply the code in a similar manner to our model cases and see if for large crack lengths and relevant displacements whether path independence holds.

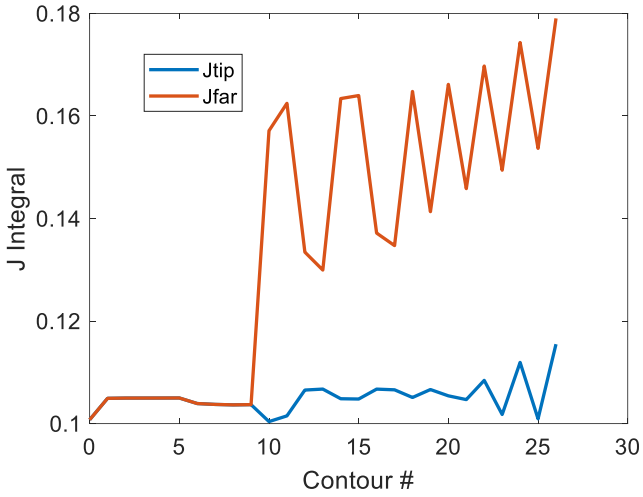

Figure 16. Path independence by considering the inhomogeneity of the interfaces

References

Shih, C.F., Moran, B., Nakamura, T., 1986. Energy release rate along a three-dimensional crack front in a thermally stressed body. International Journal of Fracture 30, 79-102.

Simha, N.K., Fischer, F.D., Kolednik, O., Predan, J., Shan, G.X., 2005. Crack Tip Shielding or Anti-shielding due to Smooth and Discontinuous Material Inhomogeneities. International Journal of Fracture 135, 73-93.